Curr Radiol Rep (2014) 2:31
DOI 10.1007/s40134-013-0031-y

OSTEOPOROSIS IMAGING (L LENCHIK, SECTION EDITOR)

Emerging Research on Bone Health Using High-Resolution CT and MRI

Hans Liebl · Thomas Baum · Dimitrios C. Karampinos · Janina Patsch · Andreas Malecki · Florian Schaff · Elena Eggl · Ernst J. Rummeny · Franz Pfeiffer · Jan S. Bauer

Published online: 27 November 2013

Abstract Today's most prevalent bone disease in the western hemisphere is osteoporosis. Predominantly postmenopausal women and older men suffer from bone loss caused by an imbalance in the physiological tissue renewal process between bone formation and resorption. As a result, osteoporosis is associated with fragility fractures, disability, impaired bone regeneration and increased mortality. The World Health Organization based the gold standard for diagnosing osteoporosis on bone mineral density (BMD) measurements using dual X-ray absorptiometry. However, BMD measurements are limited in discriminating subjects with and without osteoporotic fractures and have been shown to only partly reflect successful treatment of osteoporotic fractures. Bone microstructure is an integral determinant of bone strength. Today, new high-resolution imaging techniques such as high-resolution peripheral quantitative computed tomography and high-resolution magnetic resonance imaging make it possible to measure three-dimensional bone microarchitecture and volumetric bone mineral density with high accuracy and a relatively low radiation dose.

Keywords Osteoporosis · Multidetector computed tomography (MDCT) · Magnetic resonance imaging (MRI) · Dark field imaging · High-resolution bone imaging

This article is part of the Topical Collection on *Osteoporosis Imaging*.

H. Liebl (✉) · T. Baum · D. C. Karampinos · E. J. Rummeny
Department of Diagnostic and Interventional Radiology, Klinikum rechts der Isar, Technische Universität München, Ismaninger Str. 22, 81675 Munich, Germany
e-mail: lieblhans@gmail.com

J. Patsch
Department of Radiology, CIR (Computational Image Analysis and Radiology), Medical University of Vienna, Lazarettgasse 14, 1090 Vienna, Austria

A. Malecki · F. Schaff · E. Eggl · F. Pfeiffer
Department of Physics and Institute of Medical Engineering, Technische Universität München, Boltzmannstraße 11, 85748 Garching, Germany

J. S. Bauer
Department of Neuroradiology, Klinikum rechts der Isar, Technische Universität München, Ismaninger Str. 22, 81675 Munich, Germany

Introduction

The constant process of bone remodeling is a delicate balance between bone resorption by osteoclasts and bone formation by osteoblasts, which maintains bone mass during adulthood. Osteoporosis is the most prevalent disruption of this complex system in our aging societies, and is characterized by inherent bone loss and an increased risk for fragility fractures, with sites most commonly affected being the spine, wrist and hip [1]. The poor primary stability of the fragile bone in osteoporotic fractures results in associated disability and increased mortality [2–4]. There is an ongoing discussion on whether the regenerative capacity of osteoporotic bone is likely to be additionally impaired. With unfavorable healing conditions and an increased risk for further bone fractures once a fracture has occurred, consequences are drastic [5]. The rising prevalence of osteoporosis and subsequent healthcare costs are burdens on the individual level and socioeconomically [6]. Approximately 26 % of women aged ≥65 years and over 50 % of women aged ≥85 years are affected with postmenopausal osteoporosis (PMO), and direct and associated costs are estimated to reach $12–18 billion in the US [7].

To counter these challenges, significant efforts are being made to investigate and fully understand the underlying etiopathology, a complex interplay of metabolic factors and local tissue dynamics that exceed the compartmental boundaries of the bone.

Accurate diagnosis and effective monitoring to evaluate treatment response are crucial. The World Health Organization (WHO) based their diagnostic standard on bone mineral density measurements (BMD) using dual X-ray absorptiometry (DXA). Quantitative computed tomography (QCT) is another common alternative to quantify BMD. Both techniques compare individual values of bone density expressed as grams of mineral per area or volume to the peak bone mass of a reference cohort. However, these quantitative measurements may insufficiently assess bone health, as biomechanical strength depends on bone quality parameters that may not be mirrored by density. Trabecular and cortical microarchitecture, turnover, damage (e.g., microfractures) and mineralization play crucial roles in bone stability. Consequently, these additional parameters have been investigated to further investigate fracture probability. The WHO population-based fracture risk assessment tool (FRAX) [8] integrates clinical risk factors to calculate the 10-year fracture probability, but does not include bone strength and quality parameters [9]. Furthermore, the FRAX algorithm was shown to perform poorly in men with osteoporosis [10]. High-resolution imaging provides visualization of the cortical and trabecular bone microstructure and its three-dimensional rod- and plate-like constituents, which have a size of approximately 50–200 μm, allowing assessment of bone quality.

Various imaging techniques have been introduced to non-invasively evaluate bone architecture, such as micro computed tomography (μCT) systems, high-resolution peripheral quantitative computed tomography (HR-pQCT), high-resolution multidetector computed tomography (MDCT) and high-resolution magnetic resonance imaging (MRI). Furthermore, bone structure may be further analyzed with novel modalities such as quantitative ultrasound (QUS) and dark field imaging, which are currently under investigation.

Techniques

Standard Techniques

The diagnostic gold standard for osteoporosis as defined by the WHO has been based on the measurement of BMD. Usually two skeletal sites are measured using DXA, typically the lumbar spine and the proximal femur [11]. DXA measurements are well established and accurate, but do not differentiate cortical and trabecular bone and do not reflect bone quality parameters well [12•]. Computed tomography (CT) uses reconstructed image intensity values representing the local X-ray attenuation. It allows for excellent three-dimensional image contrast between soft and mineralized tissues. Standard clinical CT scanner systems equipped with reference phantoms containing objects of known hydroxyapatite concentrations for quantitative calibration can be used to assess BMD with quantitative CT (QCT; Fig. 1). QCT permits separate characterization of the trabecular and the cortical bone compartment, which are usually analyzed in the lumbar vertebral bodies, L1–L3. Trabecular QCT values can be interpreted similarly as DXA results using reference cohorts. Average values below 80 mg hydroxyapatite/cm^3 are considered a diagnosis of osteoporosis, whereas values between 80 and 120 mg hydroxyapatite/cm^3 indicate osteopenia [13]. However, QCT fails to explain the disparity found between bone density and bone microarchitecture in assessing fragility fracture risk: BMD has been shown to account for approximately 70–75 % of bone strength, but the remaining effect seems to be associated to other factors such as bone architecture, tissue composition and trauma [14]. Saito et al. [15•] recently suggested reduced collagen cross-linking as a potential explanation for reduced bone strength despite normal BMD in diabetics. Furthermore, therapeutic effects are also insufficiently reflected by changes in BMD: studies investigating surrogate markers for bone strength

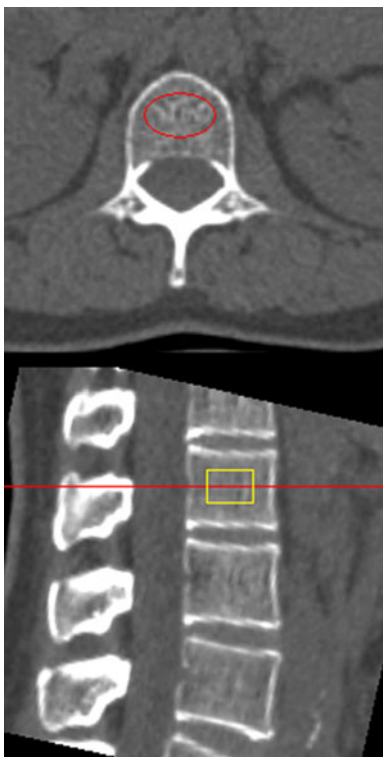

Fig. 1 QCT images (*top*: axial; *bottom*: sagittal) of the lumbar spine showing ROIs for BMD quantification

concluded that DXA-derived BMD is limited in predicting fractures, indicating the need to identify the parameters associated with fracture risk [16, 17].

High-Resolution CT Imaging Modalities

Microarchitecture has been described to be a significant contributor to bone strength. Substance loss, trabecular thinning, but also modified trabecular topology, such as the change of plate-like trabeculae into rod-shaped trabeculae and the loss of trabecular connectivity, result in the loss of bone stability. The deterioration of cortical structures also seems to contribute to increased fracture risk. Different modalities based on CT technology are currently in use to acquire high-resolution bone images evaluating microarchitecture: μCT, HR-pQCT and MDCT. Bone trabeculae have a diameter between about 50–200 μm, and the cortical bone presents with a thickness between 0.2 and 5 mm. Therefore, spatial resolution is the limiting factor of any system to perform microstructure analysis.

Micro computed tomography (μCT) is a high-resolution technique limited to in vitro studies. Small invasively harvested bone biopsy cores from the iliac crest can be analyzed with an isotropic voxel size below 8 μm to depict trabecular microstructure [18]. However, there are significant disadvantages due to the invasiveness and small sample size, which are usually harvested from locations not affected by fractures. Eckstein et al. [19] demonstrated that morphological and mechanical properties vary among anatomical locations, indicating site-specific patterns of trabecular microarchitecture. Site-specific measurements at adequate anatomical locations may therefore be less heterogeneous and more precise in predicting fracture risk. In vitro and in vivo studies have shown that fracture risk is assessed better by a combination of structural parameters and BMD derived from site-specific high-resolution imaging modalities [20–22].

High-Resolution Peripheral Quantitative CT

Since the year 2000, HR-pQCT devices have become commercially available, specifically designed for the imaging of bone microstructure in the peripheral skeleton. HR-pQCT enables a non-invasive, low-radiation assessment of bone providing information on the microarchitecture and volumetric BMD in cortical and trabecular compartments of the distal radius and distal tibia [23]. Currently, one manufacturer dominates the market for commercially available scanners performing at a resolution sufficient to analyze human bone microarchitecture in vivo (SCANCO Medical AG, Brüttisellen, Switzerland). HR-pQCT allows for a significantly higher SNR and spatial resolution compared to MDCT and MRI with an isotropic spatial resolution of 82 μm^3 (the actual spatial resolution is approximately 130 μm near the center of the field of view) in vivo with relatively low effective radiation doses of approximately 4 μSv per scan, a dose that is several orders of magnitude lower compared to whole body CT [24]. A great benefit of HR-pQCT is the possibility for morphometric analysis similar to classical histomorphometry, calculated from the binary trabecular bone images [25]. To permit data interpretation, normative databases providing reference for bone microarchitecture data had to be established enabling population-based comparisons of individual measurements: the Calgary cohort of the (CaMOS) cohort, the Rochester, Minnesota, cohort and the Cambridge, UK, cohort [26, 27]. Unlike MRI and MDCT, which are limited by a large slice thickness compared to their in-plane resolution, HR-pQCT enables direct measurements of microarchitecture parameters in a fairly large bone volume and can be paired with computer-based finite element analysis modeling (FEM) for non-invasive assessment of fracture risk. HR-pQCT has been shown to be able to differentiate between women and men with and without fractures and has increased our understanding of bone architecture and its structural changes related to age, gender, various metabolic disorders and in response to drug therapies [27–30].

Due to high acquisition and maintenance costs and the need for regular phantom calibration, only few systems are clinically used, and currently most scanners are found at research institutions. This is in part because the relatively long scan times (approximately 3 min) frequently result in motion artifacts. Furthermore, the technique is limited to the evaluation of extremities, providing no information about the more central sites commonly affected by osteoporotic fragility fractures.

Multidetector CT

Multidetector CT is routinely applied in clinical practice, but to achieve adequate spatial resolution at central regions of the skeleton, considerable radiation doses are required, limiting the technique's applicability in vivo. Studies examining vertebral microstructure using high-resolution MDCT reported estimated effective doses in the range of 3 mSv, compared to an exposure of approximately 0.1–0.3 mS delivered through a standard QCT of the lumbar spine [31]. However, the radiation doses can be significantly reduced using novel iterative reconstruction algorithms [32, 33]. Baum et al. [20] have demonstrated in a study conducted on 187 proximal femur specimens that models combining DXA and MDCT-derived trabecular bone structure parameters performed better at predicting failure load than DXA alone. Furthermore, FEMs from in vivo MDCT spine images have been shown to reliably

assess bone strength and to differentiate subjects with and without fragility fractures better than BMD measurements alone [22, 34]. In studies measuring the vertebral bone strength assessing the therapeutic effects of teriparatide, alendronate and risedronate, MDCT-based FEMs (as shown below) also provided more information than BMD measurements alone [35, 36].

Magnetic Resonance Imaging

Bone tissue contains relatively low numbers of protons and consequently yields low MR signal, appearing dark in most clinically used sequences. The MR signal of bone marrow on the contrary is relatively high, depending on the fat content and the sequence used. Therefore, bone structures can be well contrasted against the background fatty marrow signal, and information on the microarchitecture of the bone can be extracted from the acquired data. MRI lacks ionizing radiation, but has mainly been used to evaluate the peripheral skeletal sites such as the radius and tibia (Fig. 2). A resolution with voxel sizes of up to 137 × 137 × 410 μm^3 has been reported at the radius [37, 38]. Spatial resolution and image quality highly depend on the field strength, the coils and the sequence used. MRI-derived trabecular bone structure parameters have been shown to be superior to MDCT in assessing bone strength [39] and performed particularly well at high filed strength [40]. Different from MDCT, there is no direct linear relationship between tissue signal and mineralization of the bone. Thus, advanced post-processing for quantification and standardization has to be applied. Furthermore, the interdependency of SNR and spatial resolution has not been fully clarified, and studies have suggested systematic changes in the extracted structural parameters that may be normalized using linear transformations [41]. However, other studies claim that these errors may be SNR-independent for large ranges [42].

MR-based structural parameters of the radius have been shown to improve the prediction of radial bone strength, outperforming DXA-derived BMD [43]. With the more widespread use of high-field MRI and progress in sequence and coil development, previous limitations of deeper body locations such as low SNR and radio frequency signal attenuation by surrounding tissue can now be overcome [44]. Studies have shown promising results, but evaluation of common fracture sites such as the proximal femur remains challenging because of the presence of hematopoietic bone marrow [21]. Annihilating the positive background contrast of fatty bone marrow with its dark signal, hematopoietic marrow limits the visualization of the trabeculae. Its content in vertebral bodies is even higher, resulting in insufficient contrast to depict microstructures. Additional bone marrow quantification using MR spectroscopy to evaluate bone marrow fat content may complement osteoporosis imaging [45, 46]. A study by Wehrli et al. [47] demonstrated that MRI-based trabecular bone structure parameters provide a promising tool to evaluate structural treatment responses. The parameters revealed drug effects partly not captured by BMD measurements, indicating feasibility to monitor osteoporosis therapy. Chestnut et al. [48] showed similar results of successful osteoporotic treatment monitoring at the radius using MRI-based trabecular bone structure parameters.

Parameters to quantify bone structure

To identify the cortical and trabecular bone compartments, regions of interest (ROIs) usually have to be defined first, and images for longitudinal studies need to be registered to minimize reproducibility errors. Various structural parameters have been investigated to assess bone microstructure: scale parameters, represented by bone volume, thickness of the trabeculae and the spaces in between; topological parameters differentiating plate- and rod-like trabeculae, and orientation parameters characterizing the amount of anisotropy within the depicted volume. Standard structural parameters can be computed from both MDCT and MR images similar to classic bone histomorphometry [49, 50]: bone volume divided by total volume (BV/TV; bone volume fraction), trabecular number (Tb.N), trabecular separation (Tb.Sp) and trabecular thickness (Tb.Th) [51].

Based on the two peaks of the signal intensity histogram of high-resolution images and a set threshold discriminating bone and marrow voxel values, the number of bone voxels and total voxels within an ROI can be extracted. If partial volume effects merge the two distinct peaks of the intensity histogram, binarization of the image into bone and bone marrow using an empirically defined threshold becomes necessary (Fig. 3). Commonly an optimized, global threshold is chosen for CT images to avoid overestimation of bone volume in subjects with dense trabecular bone or underestimation in osteoporotic subjects. Bauer et al. [52] and Baum et al. [20] suggested a global threshold of 200 mg hydroxyapatite/cm^3 on femur specimens. MR images have also been binarized for trabecular bone structure analysis using the signal intensity of the cortical bone in MR images as a reference, as published by Majumdar et al. [53]. Changing thresholds for image binarization can significantly influence the measured values of trabecular bone structure parameters in MDCT and MR images as they vary because of partial-volume effects and subsequent SNR changes. Because of limited spatial resolution, MDCT and MRI structure parameters cannot depict the true trabecular structure, and measures are therefore labeled as apparent values. Krug et al. [54] have proposed a

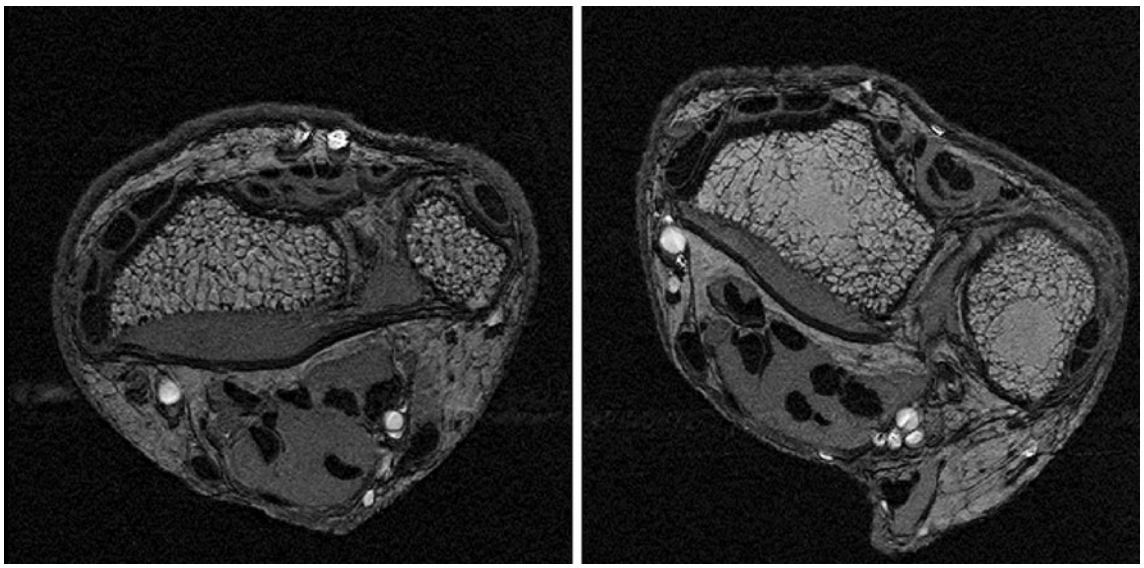

Fig. 2 Representative MR images of the forearm of a healthy (*left*) and osteoporotic (*right*) patient acquired by using a three-dimensional gradient echo sequence (in-plane resolution 195 × 195 μm^2, axial slice thickness 500 μm) at 1.5 T

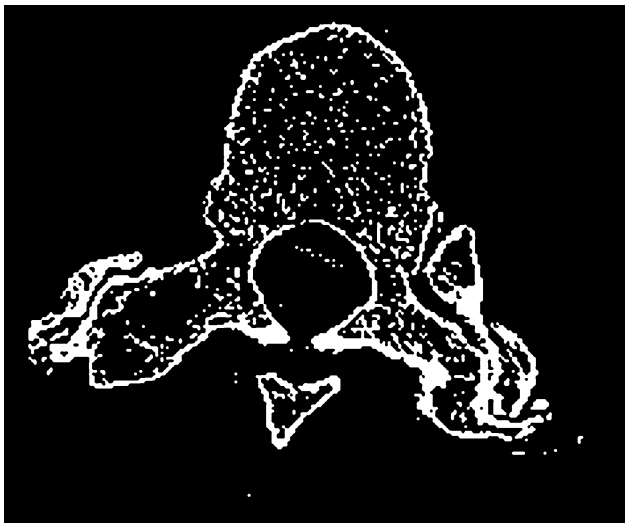

Fig. 3 Binarized axial image of a lumbar vertebral body derived from MDCT

3D approach without the need for image binarization: By computing 3D trabecular bone thickness maps, the number of pixels with thickness values different from zero can be counted and divided by the total number of pixels in the volume.

Furthermore, alternative trabecular structure parameters that do not require a threshold have been suggested, such as fuzzy logic [55, 56], the scaling index method [57] and geodesic topological analysis [58]. The scaling index method analyzes the geometry of each voxel and whether they are rod-like or plate-like structures (Fig. 4). Mueller et al. [59] demonstrated the scaling index method significantly improves diagnostic performance, differentiating postmenopausal women with and without osteoporotic vertebral fractures. Saha et al. [60] introduced a fuzzy distance transformation, and Carballido-Gamio and coworkers [55] introduced fuzzy clustering analysis for trabecular bone analysis, based on the principle that voxels can be both part of the bone compartment and of the marrow compartment at the same time. Lastly, geodesic topological analysis assesses the topology and anisotropy of the trabecular bone network without binarizing the image, based on the fact that osteoporosis is characterized by increased fenestration of trabecular plates and connectivity loss [58]. Aside from the aforementioned morphometric parameters, additional parameters such as fabric [61], a trabecular anisotropy measurement, texture parameters derived from binarized images [62] and Minkowski functionals [63] as non-linear topological parameters evaluating volume, surface area, mean integral curvature and Euler characteristics have been described.

Cortical bone can also be evaluated separately: averages of the cortical thickness (in mm), cross-sectional area (mm^2), length (mm) and surface (mm^2) can be calculated [64, 65]. More recently, the evaluation of cortical porosity has gained attention, which has been shown to be a promising parameter of cortical stability derived from HR-pQCT [66]. By influencing the mechanical properties of cortical bone, it may serve as an indicator for osseous changes related to metabolic disease. In a study on postmenopausal women with and without fragility fractures, Patsch et al. [67•] recently demonstrated that diabetic women with fragility fractures showed greater intracortical pore volume, cortical thinning and cortical porosity than diabetic women without fractures (Fig. 5). However, at

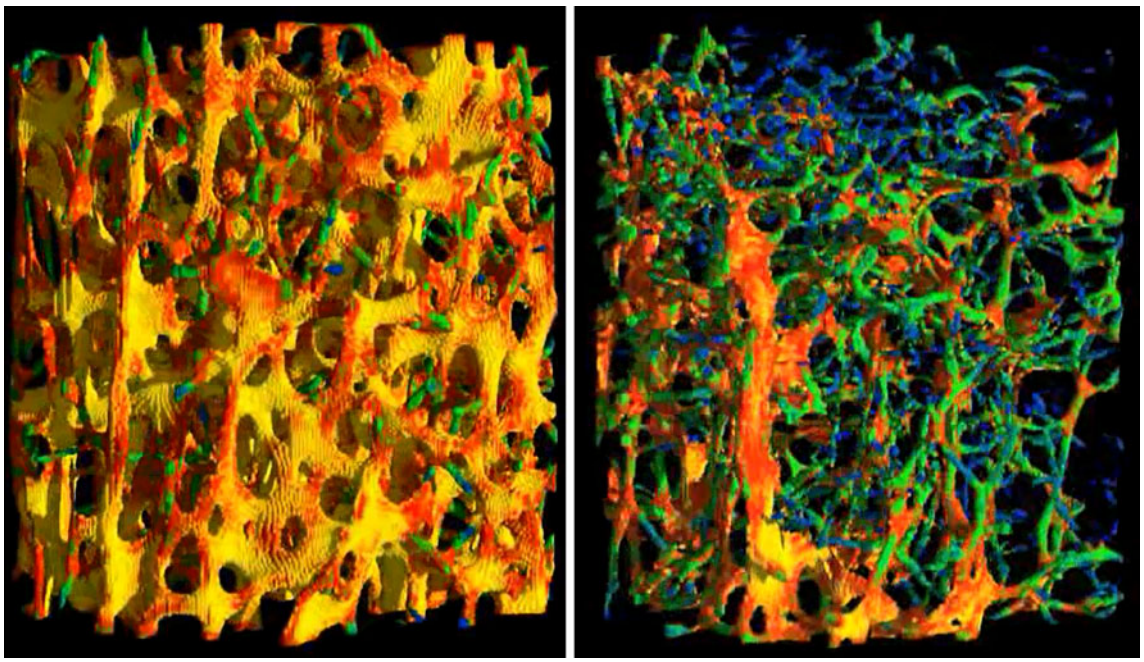

Fig. 4 Representative micro-CT images of bone samples from a healthy (*top*) and an osteoporotic (*bottom*) donor demonstrating the color-coded visualization of the scaling index α representing the local dimensionality, which is increasing from *blue* over *green* to *red* color (Color figure online)

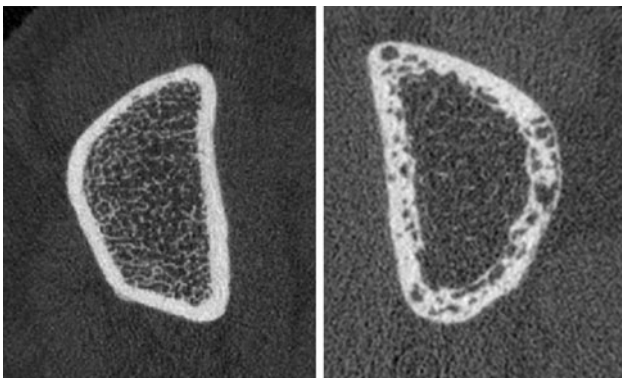

Fig. 5 Images derived from HR-pQCT demonstrating healthy trabecular and cortical bone structures (*left*) compared to a woman with type 2 diabetes showing increased cortical porosity and reduced trabecular microarchitecture. Images courtesy of Janina Patsch, University of California, San Francisco, CA, USA

present cortical porosity cannot be assessed in clinical MDCT because of limited spatial resolution. Goldenstein et al. [68] investigated intracortical porosity using MRI compared to HR-pQCT: Cortical porosity did not vary greatly between the subjects analyzed, but different types of cortical pores with varying content were found.

Finite Element Modeling (FEM)

An alternative to the structure measurements described above to evaluate bone strength is to calculate elastic and shear moduli using finite element models (FEM). FEMs can be computed within defined ROIs of trabecular or cortical bone, or for both compartments combined, based on 3D data from HR-pQCT, MDCT and MRI [69–71]. FEMs are based on the volumetric distribution of density parameters and bone geometry. Loading conditions are then implemented into the model, simulating either static loading conditions or a localized impact caused by a fall to the side, e.g., the greater trochanter of the femur. Various types of FEMs have been used. FEMs of the spine and proximal femur have been studied based on MDCT images [69]. Furthermore, micro-FEMs (μFEMs) have been computed from in vivo MR images [72]. Extensive computational power and post-processing resources are needed to perform the complex processing, and in some cases interpolation to higher apparent resolution is required. So far, FEM and μFEM analyses have been mainly limited to research institutions, but hardware and software improvements allow for future clinical application. Recent advancements, such as the new p-version and the finite cell method, have improved the h-version simulation algorithm, providing more accurate prediction of bone stability.

Current Trends and Future Developments

Both clinical MDCT and MRI so far have failed to provide true bone microstructure because of insufficient spatial resolution and low SNR in areas with red bone marrow in MRI. However, microarchitecture and structural parameters obtained by MDCT and MRI have been shown to be highly

Fig. 6 Comparison of μCT image (resolution: 8 μm isotropic) with images derived from MDCT (resolution: 0.2 × 0.2 × 0.5 mm^3) and MDCT with soft tissue simulation at the hip

correlated to μCT and HR-pQCT measurements and to predict bone strength determined by FEM similarly well [38, 73]. Bauer et al. [74] used 20 cylindrical trabecular bone specimens harvested from formalin-fixed human thoracic spine vertebrae and obtained μCT images (isotropic voxel size: 20 μm^3) as well as corresponding MDCT images with a voxel size of up to 230 × 230 × 500 μm^3. Comparison of trabecular bone structure parameters obtained from μCT and MDCT (Fig. 6) showed R^2 values up to 0.84. In addition, trabecular bone structure parameters derived from MDCT were highly correlated with biomechanical properties derived from FEM analysis (R^2 values up to 0.81). Images of a spine specimen acquired with MDCT and HR-pQCT as standard of reference (Fig. 7). Similar results were presented for specimens harvested from the calcaneus by Diederichs et al. [75]. Issever et al. [76] compared the performance of 64- and 320-slice MDCT scanners for the depiction of trabecular bone architecture and found no statistically significant differences.

MRI-derived structural measures also demonstrated high accordance with μCT. Krug et al. [77] used ex vivo and in vivo peripheral trabecular bone structure parameters derived from 3-T MRI compared to HR-pQCT as standard of reference. Eight human specimens and 11 volunteers were imaged with both modalities at a voxel size of 156 × 156 × 500 μm^3 at 3 T MRI and 82 μm^3 at HR-pQCT. MRI- and HR-pQCT-derived bone structure parameters showed high compliance ($R^2 > 0.8$). Another study conducted by Phan et al. [40] investigated trabecular bone structure parameters at the calcaneus derived from in vitro μCT compared to 1.5- and 3-T MRI. The correlation of bone microstructure parameters derived from gradient echo sequences at 3-T MRI with μCT measures was higher than the association between bone structure parameters obtained at 1.5-T MRI and μCT measurements.

SNR increase and spatial resolution at high field strengths are a trade-off, and larger susceptibility effects alter the structural measurements because of artificially thickened trabeculae. Krug et al. investigated the impact of SNR on bone imaging using high-field MRI and found a significant SNR increase at 7 T [78]. Baum et al. [79] found similar reproducibility errors at 1.5- and 3-T MRI, but absolute parameter values were significantly different, so it remains questionable whether microarchitecture parameters derived from 3- and 1.5-T MRI are comparable.

Various novel imaging techniques and continuous refinement of conventional hardware as well as software and post-processing algorithms enrich our understanding of bone health, pushing the boundaries of imaging resolution and functional quantification. A new generation of flat panel scanners has been introduced, combining standard MDCT gantries with two-dimensional flat panel detectors allowing for fast continuous acquisitions at high spatial resolution [80, 81]. Iterative reconstruction algorithms may allow for radiation dose reduction of clinical MDCT without compromising the resolution of trabecular and cortical structures.

Quantitative Ultrasound

Quantitative ultrasound has emerged as a promising technique without ionizing radiation, and QUS-based measurements have been shown to be highly correlated with BMD: Phalangeal bone structure has been shown to influence the velocity (SoS), shape (number of peaks) and amplitude of the ultrasound signal [82–84]. QUS parameters measured are bone transmission time (BTT) and pure speed of sound (pSoS). QUS was shown to perform well in fracture risk prediction, and based on QUS measurements, subjects with and without spine and hip fractures could be differentiated [85, 86]. Ingle et al. [87] have demonstrated good precision over time for the follow-up monitoring of osteoporosis therapies with different drugs such as alendronate and oestradiol. Unfortunately, QUS is limited

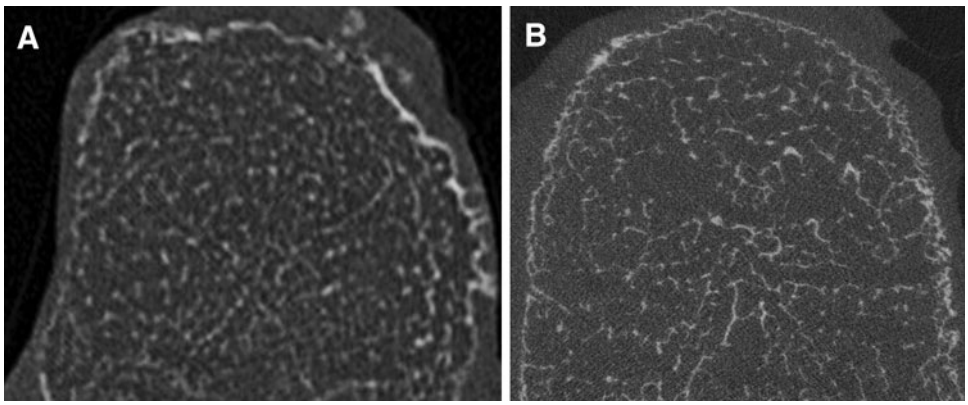

Fig. 7 Corresponding MDCT (**a**) and HR-pQCT (**b**) images of a spinal segment unit spatial resolution: 250 × 250 × 600 μm^3 versus 41 μm^3

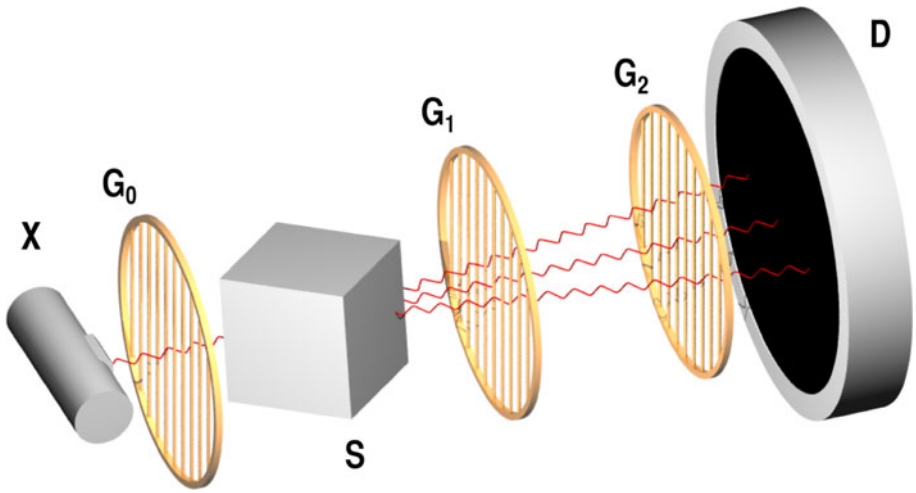

Fig. 8 Sketch of a typical X-ray grating interferometry setup. X-ray tube (X) and detector (D) encasing the sample (S) placed between three gratings (G0, G1, G2), which are required to extract the three different contrast types: attenuation contrast, phase contrast and dark-field contrast

to peripheral sites (the radius, tibia, calcaneus and the phalanx are currently being studied), and the clinically most important fracture sites (spine and hip) cannot be evaluated directly [88].

Phase-Contrast and X-Ray Dark-Field Imaging

Recently, it has been shown that complementary conventional X-ray contrast modalities such as phase-contrast and dark-field contrast may be applied in a clinical environment [89•]. Phase-contrast imaging has been shown to be a sensitive soft tissue imaging modality. Dark-field contrast however may have great potential in bone imaging, providing additional information about the micro-morphology. Dark-field imaging is based on the physical process of scattering at features in the micrometer range. Without resolving the individual features directly, it allows drawing conclusions about the number of structures, their size and their anisotropy [90]. In addition to plain acquisitions, tomography can also be performed [91].

One commonly used experimental setup requires a so-called Talbot-Lau interferometer, consisting of three grating structures with periods in the μm range (Fig. 8). A first grating ensures that coherence requirements are met. It is followed by two absorbing gratings, which introduce a periodic phase shift to the incoming x-ray beam. The phase shift is then converted into an intensity modulation using the so-called fractional Talbot effect, which is analyzed with the last grating. By moving the gratings, detector images can be recorded for different positions, allowing for the extraction of three registered distinct contrast channels from each data set [90, 92].

Several proof-of-principle studies have been conducted investigating the dark-field signal in the presence of emphysema [93], contrast agents [94] and micro-calcifications [95]. As the grating interferometer is only sensitive to scattering perpendicular to the grating lines, local structure orientation can be deduced: Representative directional dark-field images (DDFI), also termed X-ray vector radiographs (XVR) (Fig. 9). They demonstrate the color-coded orientation of trabecular structures for different projections of a femoral trabecular bone cube. Directional dark-field imaging techniques are potentially useful for analyzing the osseous microarchitecture and compatible with standard clinical devices. However, future studies have to demonstrate technical feasibility with a limited

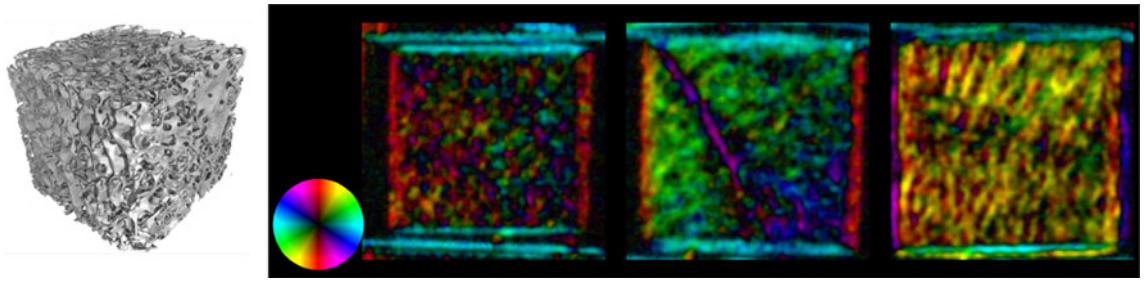

Fig. 9 XVR images of a femoral bone sample. The *cubic* specimen is shown on the *left*. The XVR images were taken along the three surface normals. The color encodes the local orientation, and the brightness corresponds to the anisotropy of the scattering signal. Structures perpendicular to the bulk cause a change in direction of the scattering signal by 90°. A signal deviation indicated by the change in color compared to the surrounding areas caused by the epiphyseal plate is demonstrated in the second image to the *right* (Color figure online)

radiation dose and clinical benefits extending beyond those of MDCT.

Conclusion

In the recent years, progress in high-resolution bone imaging has been tremendous. CT and MRI systems are widespread in clinical practice and are therefore potentially available for bone microstructure analyses. Bone microarchitecture parameters and finite element model data derived from high-resolution CT images, MDCT data and MR images have improved the assessment of trabecular and cortical bone architecture beyond BMD measurements, allowing for more accurate diagnosis with limited radiation exposure. In addition, microstructure parameters have been shown to be more sensitive to structural changes associated with pharmacotherapy effects compared to BMD measurements alone and thus may also be more effective in monitoring treatment.

Newly developed hardware, advancements in image post-processing, MRI scanners with high field strengths of up to 7 T in combination and newly developed software such as UTE sequences create new promising possibilities in evaluating bone microstructure of both trabecular and cortical bone compartments also at more central body sites. HR-pQCT provides in vivo images with extremely high resolution from peripheral sites at short acquisition times. Novel reconstruction algorithms using iterative reconstruction may allow for reliable assessment of trabecular bone at decreased radiation dose levels with MDCT imaging, and new flat panel scanners are available.

In conclusion, high-resolution bone imaging is crucial for the investigation of bone disease and the underlying etiopathologies.

Acknowledgments We acknowledge financial support from the Deutsche Forschungsgemeinschaft (DFG) Cluster of Excellence Munich-Centre for Advanced Photonics (MAP), the DFG Gottfried Wilhelm Leibniz program and the European Research Council (ERC, FP7, StG 240142). This work was supported in parts by grants of the Deutsche Forschungsgemeinschaft (DFG BA 4085/1-2).

Compliance with Ethics Guidelines

Conflict of Interest Hans Liebl, Thomas Baum, Dimitrios C. Karampinos, Janina Patsch, Andreas Malecki, Florian Schaff, Elena Eggl, Ernst J. Rummeny, Franz Pfeiffer and Jan S. Bauer declare no conflicts of interest.

Human and Animal Rights and Informed Consent This article does not contain any studies with human or animal subjects performed by any of the authors.

References

Papers of particular interest, published recently, have been highlighted as:
- Of importance

1. Schousboe JT, Fink HA, Taylor BC, et al. Association between self-reported prior wrist fractures and risk of subsequent hip and radiographic vertebral fractures in older women: a prospective study. J Bone Miner Res. 2005;20(1):100–6.
2. Boonen S, Autier P, Barette M, et al. Functional outcome and quality of life following hip fracture in elderly women: a prospective controlled study. Osteoporos Int. 2004;15(2):87–94.
3. Papaioannou A, Kennedy CC, Ioannidis G, et al. The impact of incident fractures on health-related quality of life: 5 years of data from the Canadian Multicentre Osteoporosis Study. Osteoporos Int. 2009;20(5):703–14.
4. Jalava T, Sarna S, Pylkkanen L, et al. Association between vertebral fracture and increased mortality in osteoporotic patients. J Bone Miner Res. 2003;18(7):1254–60.
5. Ioannidis G, Papaioannou A, Hopman WM, et al. Relation between fractures and mortality: results from the Canadian Multicentre Osteoporosis Study. CMAJ. 2009;181(5):265–71.
6. Burge R, Dawson-Hughes B, Solomon DH, et al. Incidence and economic burden of osteoporosis-related fractures in the United States, 2005-2025. J Bone Miner Res. 2007;22(3):465–75.
7. Parthan A, Kruse M, Yurgin N, et al. Cost effectiveness of denosumab versus oral bisphosphonates for postmenopausal osteoporosis in the US. Appl Health Econ Health Policy. 2013;11(5):485–97.

8. WHO Study Group. Assessment of fracture risk and its application to screening for postmenopausal osteoporosis. Report of a WHO Study Group. World Health Organ Tech Rep Ser. 1994;843:1–129.
9. Goodhand JR, Kamperidis N, Nguyen H, et al. Application of the WHO fracture risk assessment tool (FRAX) to predict need for DEXA scanning and treatment in patients with inflammatory bowel disease at risk of osteoporosis. Aliment Pharmacol Ther. 2011;33(5):551–8.
10. Sandhu SK, Nguyen ND, Center JR, et al. Prognosis of fracture: evaluation of predictive accuracy of the FRAX algorithm and Garvan nomogram. Osteoporos Int. 2010;21(5):863–71.
11. Li N, Li XM, Xu L, et al. Comparison of QCT and DXA: osteoporosis detection rates in postmenopausal women. Int J Endocrinol. 2013;2013:895474.
12. • Graeff C, Marin F, Petto H, et al. High resolution quantitative computed tomography-based assessment of trabecular microstructure and strength estimates by finite-element analysis of the spine, but not DXA, reflects vertebral fracture status in men with glucocorticoid-induced osteoporosis. Bone. 2013;52(2):568–77. *Graeff et al. conducted the first study in which MDCT was used to study not only bone forming but also antiresorptive treatment. CT-based FE analysis estimating vertebral strength showed highly consistent results for vertebral strength improvement under therapy demonstrating effective monitoring of therapeutic drug effects, which were more sensitive than BMD measurements derived from DXA.*
13. Hain SF. DXA scanning for osteoporosis. Clin Med. 2006;6(3):254–8.
14. NIH Consensus Development Panel on Osteoporosis. NIH Consensus Development Panel on osteoporosis prevention, diagnosis, and therapy, March 7–29, 2000: highlights of the conference. South Med J. 2001;94(6):569–73.
15. • Saito M, Marumo K. Bone quality in diabetes. Front Endocrinol (Lausanne). 2013;4:72. *Saito et al. provide evidence to suggest that advanced glycation end products (AGEs) could explain the molecular link between primary osteoporosis and diabetes. This may help to explain why type 2 diabetes is characterized by normal or high BMD, but is associated with an increased risk of fracture.*
16. Black DM, Thompson DE, Bauer DC, et al. Fracture risk reduction with alendronate in women with osteoporosis: the fracture intervention trial. FIT Research Group. J Clin Endocrinol Metab. 2000;85(11):4118–24.
17. Vestergaard P. Discrepancies in bone mineral density and fracture risk in patients with type 1 and type 2 diabetes—a meta-analysis. Osteoporos Int. 2007;18(4):427–44.
18. Palacio-Mancheno PE, Larriera AI, Doty SB, et al. 3D assessment of cortical bone porosity and tissue mineral density using high-resolution micro-CT: Effects of resolution and threshold method. J Bone Miner Res. 2013. doi:10.1002/jbmr.2012.
19. Eckstein F, Matsuura M, Kuhn V, et al. Sex differences of human trabecular bone microstructure in aging are site-dependent. J Bone Miner Res. 2007;22(6):817–24.
20. Baum T, Carballido-Gamio J, Huber MB, et al. Automated 3D trabecular bone structure analysis of the proximal femur—prediction of biomechanical strength by CT and DXA. Osteoporos Int. 2010;21(9):1553–64.
21. Link TM, Vieth V, Langenberg R, et al. Structure analysis of high resolution magnetic resonance imaging of the proximal femur: in vitro correlation with biomechanical strength and BMD. Calcif Tissue Int. 2003;72(2):156–65.
22. Dall'Ara E, Pahr D, Varga P, et al. QCT-based finite element models predict human vertebral strength in vitro significantly better than simulated DEXA. Osteoporos Int. 2012;23(2):563–72.
23. Boutroy S, Van Rietbergen B, Sornay-Rendu E, et al. Finite element analysis based on in vivo HR-pQCT images of the distal radius is associated with wrist fracture in postmenopausal women. J Bone Miner Res. 2008;23(3):392–9.
24. Burghardt AJ, Buie HR, Laib A, et al. Reproducibility of direct quantitative measures of cortical bone microarchitecture of the distal radius and tibia by HR-pQCT. Bone. 2010;47(3):519–28.
25. Parfitt AM, Drezner MK, Glorieux FH, et al. Bone histomorphometry: standardization of nomenclature, symbols, and units. Report of the ASBMR Histomorphometry Nomenclature Committee. J Bone Miner Res. 1987;2(6):595–610.
26. Tenenhouse A, Joseph L, Kreiger N, et al. Estimation of the prevalence of low bone density in Canadian women and men using a population-specific DXA reference standard: the Canadian Multicentre Osteoporosis Study (CaMos). Osteoporos Int. 2000;11(10):897–904.
27. Boutroy S, Bouxsein ML, Munoz F, et al. In vivo assessment of trabecular bone microarchitecture by high-resolution peripheral quantitative computed tomography. J Clin Endocrinol Metab. 2005;90(12):6508–15.
28. Liu XS, Wang J, Zhou B, et al. Fast trabecular bone strength predictions of HR-pQCT and individual trabeculae segmentation-based plate and rod finite element model discriminate postmenopausal vertebral fractures. J Bone Miner Res. 2013;28(7):1666–78.
29. Hansen S, Hauge EM, Beck Jensen JE, et al. Differing effects of PTH 1-34, PTH 1-84, and zoledronic acid on bone microarchitecture and estimated strength in postmenopausal women with osteoporosis: an 18-month open-labeled observational study using HR-pQCT. J Bone Miner Res. 2013;28(4):736–45.
30. Burghardt AJ, Lee CH, Kuo D, et al. Quantitative in vivo HR-pQCT imaging of 3D wrist and metacarpophalangeal joint space width in rheumatoid arthritis. Ann Biomed Eng. 2013. doi:10.1007/s10439-013-0871-x.
31. Graeff C, Timm W, Nickelsen TN, et al. Monitoring teriparatide-associated changes in vertebral microstructure by high-resolution CT in vivo: results from the EUROFORS study. J Bone Miner Res. 2007;22(9):1426–33.
32. Hou Y, Liu X, Xv S, et al. Comparisons of image quality and radiation dose between iterative reconstruction and filtered back projection reconstruction algorithms in 256-MDCT coronary angiography. Am J Roentgenol. 2012;199(3):588–94.
33. Mueck FG, Michael L, Deak Z, et al. Upgrade to iterative image reconstruction (IR) in MDCT imaging: a clinical study for detailed parameter optimization beyond vendor recommendations using the adaptive statistical iterative reconstruction environment (ASIR) Part2: the chest. Rofo. 2013;185(7):644–54.
34. Imai K, Ohnishi I, Yamamoto S, et al. In vivo assessment of lumbar vertebral strength in elderly women using computed tomography-based nonlinear finite element model. Spine (Phila Pa 1976). 2008;33(1):27–32.
35. Chevalier Y, Quek E, Borah B, et al. Biomechanical effects of teriparatide in women with osteoporosis treated previously with alendronate and risedronate: results from quantitative computed tomography-based finite element analysis of the vertebral body. Bone. 2010;46(1):41–8.
36. Imai K, Ohnishi I, Matsumoto T, et al. Assessment of vertebral fracture risk and therapeutic effects of alendronate in postmenopausal women using a quantitative computed tomography-based nonlinear finite element method. Osteoporos Int. 2009;20(5):801–10.
37. Ladinsky GA, Vasilic B, Popescu AM, et al. Trabecular structure quantified with the MRI-based virtual bone biopsy in postmenopausal women contributes to vertebral deformity burden independent of areal vertebral BMD. J Bone Miner Res. 2008;23(1):64–74.

38. Baum T, Kutscher M, Muller D, et al. Cortical and trabecular bone structure analysis at the distal radius-prediction of biomechanical strength by DXA and MRI. J Bone Miner Metab. 2013;31(2):212–21.
39. Link TM, Vieth V, Stehling C, et al. High-resolution MRI vs multislice spiral CT: which technique depicts the trabecular bone structure best? Eur Radiol. 2003;13(4):663–71.
40. Phan CM, Matsuura M, Bauer JS, et al. Trabecular bone structure of the calcaneus: comparison of MR imaging at 3.0 and 1.5 T with micro-CT as the standard of reference. Radiology. 2006;239(2):488–96.
41. Li CQ, Magland JF, Rajapakse CS, et al. Implications of resolution and noise for in vivo micro-MRI of trabecular bone. Med Phys. 2008;35(12):5584–94.
42. Bauer JS, Monetti R, Krug R, et al. Advances of 3T MR imaging in visualizing trabecular bone structure of the calcaneus are partially SNR-independent: analysis using simulated noise in relation to micro-CT, 1.5 T MRI, and biomechanical strength. J Magn Reson Imaging. 2009;29(1):132–40.
43. Hudelmaier M, Kollstedt A, Lochmuller EM, et al. Gender differences in trabecular bone architecture of the distal radius assessed with magnetic resonance imaging and implications for mechanical competence. Osteoporos Int. 2005;16(9):1124–33.
44. Krug R, Banerjee S, Han ET, et al. Feasibility of in vivo structural analysis of high-resolution magnetic resonance images of the proximal femur. Osteoporos Int. 2005;16(11):1307–14.
45. Tang GY, Lv ZW, Tang RB, et al. Evaluation of MR spectroscopy and diffusion-weighted MRI in detecting bone marrow changes in postmenopausal women with osteoporosis. Clin Radiol. 2010;65(5):377–81.
46. Baum T, Yap SP, Karampinos DC, et al. Does vertebral bone marrow fat content correlate with abdominal adipose tissue, lumbar spine bone mineral density, and blood biomarkers in women with type 2 diabetes mellitus? J Magn Reson Imaging. 2012;35(1):117–24.
47. Wehrli FW, Ladinsky GA, Jones C, et al. In vivo magnetic resonance detects rapid remodeling changes in the topology of the trabecular bone network after menopause and the protective effect of estradiol. J Bone Miner Res. 2008;23(5):730–40.
48. Chestnut CH 3rd, Majumdar S, Newitt DC, et al. Effects of salmon calcitonin on trabecular microarchitecture as determined by magnetic resonance imaging: results from the QUEST study. J Bone Miner Res. 2005;20(9):1548–61.
49. Issever AS, Vieth V, Lotter A, et al. Local differences in the trabecular bone structure of the proximal femur depicted with high-spatial-resolution MR imaging and multisection CT. Acad Radiol. 2002;9(12):1395–406.
50. Majumdar S, Genant HK, Grampp S, et al. Correlation of trabecular bone structure with age, bone mineral density, and osteoporotic status: in vivo studies in the distal radius using high resolution magnetic resonance imaging. J Bone Miner Res. 1997;12(1):111–8.
51. Wehrli FW, Song HK, Saha PK, et al. Quantitative MRI for the assessment of bone structure and function. NMR Biomed. 2006;19(7):731–64.
52. Bauer JS, Kohlmann S, Eckstein F, et al. Structural analysis of trabecular bone of the proximal femur using multislice computed tomography: a comparison with dual X-ray absorptiometry for predicting biomechanical strength in vitro. Calcif Tissue Int. 2006;78(2):78–89.
53. Majumdar S, Newitt D, Mathur A, et al. Magnetic resonance imaging of trabecular bone structure in the distal radius: relationship with X-ray tomographic microscopy and biomechanics. Osteoporos Int. 1996;6(5):376–85.
54. Krug R, Carballido-Gamio J, Burghardt AJ, et al. Wavelet-based characterization of vertebral trabecular bone structure from magnetic resonance images at 3 T compared with micro-computed tomographic measurements. Magn Reson Imaging. 2007;25(3):392–8.
55. Folkesson J, Carballido-Gamio J, Eckstein F, et al. Local bone enhancement fuzzy clustering for segmentation of MR trabecular bone images. Med Phys. 2010;37(1):295–302.
56. Carballido-Gamio J, Phan C, Link TM, et al. Characterization of trabecular bone structure from high-resolution magnetic resonance images using fuzzy logic. Magn Reson Imaging. 2006;24(8):1023–9.
57. Boehm HF, Raeth C, Monetti RA, et al. Local 3D scaling properties for the analysis of trabecular bone extracted from high-resolution magnetic resonance imaging of human trabecular bone: comparison with bone mineral density in the prediction of biomechanical strength in vitro. Invest Radiol. 2003;38(5):269–80.
58. Carballido-Gamio J, Krug R, Huber MB, et al. Geodesic topological analysis of trabecular bone microarchitecture from high-spatial resolution magnetic resonance images. Magn Reson Med. 2009;61(2):448–56.
59. Mueller D, Link TM, Monetti R, et al. The 3D-based scaling index algorithm: a new structure measure to analyze trabecular bone architecture in high-resolution MR images in vivo. Osteoporos Int. 2006;17(10):1483–93.
60. Saha PK, Wehrli FW. Measurement of trabecular bone thickness in the limited resolution regime of in vivo MRI by fuzzy distance transform. IEEE Trans Med Imaging. 2004;23(1):53–62.
61. Matsuura M, Eckstein F, Lochmuller EM, et al. The role of fabric in the quasi-static compressive mechanical properties of human trabecular bone from various anatomical locations. Biomech Model Mechanobiol. 2008;7(1):27–42.
62. Pothuaud L, Newitt DC, Lu Y, et al. In vivo application of 3D-line skeleton graph analysis (LSGA) technique with high-resolution magnetic resonance imaging of trabecular bone structure. Osteoporos Int. 2004;15(5):411–9.
63. Sidorenko I, Monetti R, Bauer J, et al. Assessing methods for characterising local and global structural and biomechanical properties of the trabecular bone network. Curr Med Chem. 2011;18(22):3402–9.
64. Kazakia GJ, Hyun B, Burghardt AJ, et al. In vivo determination of bone structure in postmenopausal women: a comparison of HR-pQCT and high-field MR imaging. J Bone Miner Res. 2008;23(4):463–74.
65. Gomberg BR, Saha PK, Wehrli FW. Method for cortical bone structural analysis from magnetic resonance images. Acad Radiol. 2005;12(10):1320–32.
66. Nishiyama KK, Macdonald HM, Buie HR, et al. Postmenopausal women with osteopenia have higher cortical porosity and thinner cortices at the distal radius and tibia than women with normal aBMD: an in vivo HR-pQCT study. J Bone Miner Res. 2010;25(4):882–90.
67. • Patsch JM, Burghardt AJ, Yap SP, et al. Increased cortical porosity in type 2 diabetic postmenopausal women with fragility fractures. J Bone Miner Res. 2013;28(2):313–24. *Patsch et al. conducted a study on postmenopausal diabetic (type 2) women with and without fragility fractures using DXA and micro-FEM analysis derived from HR-pQCT. Diabetic women with fractures exhibited significantly higher cortical porosity and pore-related deficits in stiffness, failure load and cortical load fraction at the ultradistal and distal tibia, and the distal radius than diabetic women without fractures.*
68. Goldenstein J, Kazakia G, Majumdar S. In vivo evaluation of the presence of bone marrow in cortical porosity in postmenopausal osteopenic women. Ann Biomed Eng. 2010;38(2):235–46.
69. Koivumaki JE, Thevenot J, Pulkkinen P, et al. Ct-based finite element models can be used to estimate experimentally measured failure loads in the proximal femur. Bone. 2012;50(4):824–9.

70. Zhang N, Magland JF, Rajapakse CS, et al. Potential of in vivo MRI-based nonlinear finite-element analysis for the assessment of trabecular bone post-yield properties. Med Phys. 2013;40(5):052303.
71. Varga P, Dall'Ara E, Pahr DH, et al. Validation of an HR-pQCT-based homogenized finite element approach using mechanical testing of ultra-distal radius sections. Biomech Model Mechanobiol. 2011;10(4):431–44.
72. Newitt DC, Majumdar S, van Rietbergen B, et al. In vivo assessment of architecture and micro-finite element analysis derived indices of mechanical properties of trabecular bone in the radius. Osteoporos Int. 2002;13(1):6–17.
73. Baum T, Grabeldinger M, Rath C, et al. Trabecular bone structure analysis of the spine using clinical MDCT: can it predict vertebral bone strength? J Bone Miner Metab. 2013. doi:10.1007/s00774-013-0465-6.
74. Bauer JS, Issever AS, Fischbeck M, et al. Multislice-CT for structure analysis of trabecular bone—a comparison with micro-CT and biomechanical strength. Rofo. 2004;176(5):709–18.
75. Diederichs G, Link TM, Kentenich M, et al. Assessment of trabecular bone structure of the calcaneus using multi-detector CT: correlation with microCT and biomechanical testing. Bone. 2009;44(5):976–83.
76. Issever AS, Link TM, Kentenich M, et al. Assessment of trabecular bone structure using MDCT: comparison of 64- and 320-slice CT using HR-pQCT as the reference standard. Eur Radiol. 2010;20(2):458–68.
77. Krug R, Carballido-Gamio J, Burghardt AJ, et al. Assessment of trabecular bone structure comparing magnetic resonance imaging at 3 Tesla with high-resolution peripheral quantitative computed tomography ex vivo and in vivo. Osteoporos Int. 2008;19(5):653–61.
78. Krug R, Carballido-Gamio J, Banerjee S, et al. In vivo ultra-high-field magnetic resonance imaging of trabecular bone microarchitecture at 7 T. J Magn Reson Imaging. 2008;27(4):854–9.
79. Baum T, Dutsch Y, Muller D, et al. Reproducibility of trabecular bone structure measurements of the distal radius at 1.5 and 3.0 T magnetic resonance imaging. J Comput Assist Tomogr. 2012;36(5):623–6.
80. Reichardt B, Sarwar A, Bartling SH, et al. Musculoskeletal applications of flat-panel volume CT. Skeletal Radiol. 2008;37(12):1069–76.
81. Gupta R, Cheung AC, Bartling SH, et al. Flat-panel volume CT: fundamental principles, technology, and applications. Radiographics. 2008;28(7):2009–22.
82. Hans D, Njeh CF, Genant HK, et al. Quantitative ultrasound in bone status assessment. Rev Rhum Engl Ed. 1998;65(7–9):489–98.
83. He YQ, Fan B, Hans D, et al. Assessment of a new quantitative ultrasound calcaneus measurement: precision and discrimination of hip fractures in elderly women compared with dual X-ray absorptiometry. Osteoporos Int. 2000;11(4):354–60.
84. Bouxsein ML, Coan BS, Lee SC. Prediction of the strength of the elderly proximal femur by bone mineral density and quantitative ultrasound measurements of the heel and tibia. Bone. 1999;25(1):49–54.
85. • Grimal Q, Grondin J, Guerard S, et al. Quantitative ultrasound of cortical bone in the femoral neck predicts femur strength: results of a pilot study. J Bone Miner Res. 2013;28(2):302–12. *Grimal et al. used quantitative ultrasound (QUS) of the femoral neck in correlation with DXA and QCT measurements to investigate the relation of QUS parameters to the geometric and material properties of the cortical shell (cortical thickness, tissue elasticity and porosity). QUS was significantly correlated with cortical QCT variables, indicating new possibilities to assess bone strength with QUS even at deep locations such as the femoral neck.*
86. Albanese CV, De Terlizzi F, Passariello R. Quantitative ultrasound of the phalanges and DXA of the lumbar spine and proximal femur in evaluating the risk of osteoporotic vertebral fracture in postmenopausal women. Radiol Med. 2011;116(1):92–101.
87. Ingle BM, Machado AB, Pereda CA, et al. Monitoring alendronate and estradiol therapy with quantitative ultrasound and bone mineral density. J Clin Densitom. 2005;8(3):278–86.
88. Guglielmi G, Adams J, Link TM. Quantitative ultrasound in the assessment of skeletal status. Eur Radiol. 2009;19(8):1837–48.
89. • Pfeiffer F, Bech M, Bunk O, et al. Hard-X-ray dark-field imaging using a grating interferometer. Nat Mater. 2008;**7**(2):134–7. *Pfeiffer et al. describe a novel technique termed dark-field imaging using conventional X-ray tubes in combination with a grating interferometer, which may potentially allow new insights into bone micro-structure, providing complementary and otherwise inaccessible structural information at the micrometer and submicrometer length scale.*
90. Jensen TH, Bech M, Bunk O, et al. Directional X-ray dark-field imaging. Phys Med Biol. 2010;55(12):3317–23.
91. Bech M, Jensen TH, Bunk O, et al. Advanced contrast modalities for X-ray radiology: phase-contrast and dark-field imaging using a grating interferometer. Z Med Phys. 2010;20(1):7–16.
92. Malecki A, Potdevin G, Biernath T, et al. Coherent superposition in grating-based directional dark-field imaging. PLoS ONE. 2013;8(4):e61268.
93. Schleede S, Meinel FG, Bech M, et al. Emphysema diagnosis using X-ray dark-field imaging at a laser-driven compact synchrotron light source. Proc Natl Acad Sci USA. 2012;109(44):17880–5.
94. Velroyen A, Bech M, Malecki A, et al. Microbubbles as a scattering contrast agent for grating-based x-ray dark-field imaging. Phys Med Biol. 2013;58(4):N37–46.
95. Michel T, Rieger J, Anton G, et al. On a dark-field signal generated by micrometer-sized calcifications in phase-contrast mammography. Phys Med Biol. 2013;58(8):2713–32.